Theor Chim Acta (1990) 77: 85–109

Theoretica Chimica Acta

The dynamical crystal field model of selective vibronic coupling in d–d spectra

A. Ceulemans and N. Bongaerts
Department of Chemistry, University of Leuven, Celestijnenlaan 200F, B-3030 Leuven, Belgium

Received August 24, 1989; received in revised form October 23, 1989/Accepted November 30, 1989

Summary. The dynamic crystal field operators, corresponding to the normal point-charge displacements in an octahedral complex are analyzed in detail. The strict equivalence of absolute versus relative coordinate treatments is established. The resulting formalism is applied to the intensity distribution in the vibronic side bands of the sharp line luminescence spectra of d^3 complexes. Thereby special attention is given to the role of spin-orbit coupling and to the elastic properties of the molecular force field. Using the closure procedure, the relative intensities of the side bands may be expressed in terms of a single dynamic crystal field parameter. These expressions provide a simple rationalization of the observed vibronic selection rules, entirely within the framework of dynamic crystal field theory.

Key words: Dynamic crystal field theory — Vibronic coupling — Vibronic selectivity — d^3 Complexes.

1. Introduction

Parity forbidden d–d bands in centrosymmetric transition-metal complexes may acquire intensity through vibronic coupling with ungerade vibrational modes. The resulting transitions are found to be based on false origins involving single quanta of the allowing vibrations. More than thirty years ago a crystal field formalism was proposed for the quantitative calculation of the associated oscillator strengths [1, 2]. Since then, several authors have contributed to the development and refinement of this formalism, and extended its use to the description of vibronic intensities for f–f transitions [3–5]. Nonetheless, in spite of its apparent simplicity, the original model continues to attract attention. Two recent applications deal with the phosphoresence spectra of d^3 ions in an

octahedral environment. On the one hand, Kupka et al. [6] have calculated the intensity distribution in the vibronic side bands of the $\Gamma_7(^2T_{2g}) \rightarrow \Gamma_8(^4A_{2g})$ emission of $ReCl_6^{2-}$ and $ReBr_6^{2-}$ ions in various cubic host crystals, while on the other hand, Acevedo and Flint [7] have concentrated on the intensities of the $^2E_g \rightarrow {}^4A_{2g}$ transition of the MnF_6^{2-} ion. Both studies are based on the same linear vibronic coupling mechanism, starting from a similar point charge approximation. However they diverge in the use of external versus internal displacement coordinates. Furthermore, both treatments suffer from the presence of errors which may give rise to considerable confusion. To clarify this issue, we intend to present here a rigorous analysis of the correct formalism, which will clearly demonstrate the equivalence of the treatments in [6] and [7]. Furthermore, this dynamic crystal field model will be applied to the well-documented observation of vibronic selectivity in the phosphorescence spectra of d^3 complexes.

2. The crystal field formalism

In this section we review the construction of the vibronic coupling operators for the odd parity modes in a ML_6 complex with O_h symmetry. At first the treatment uses the absolute displacement coordinates, defined by Kupka et al. [6]. Next the operators are rewritten in relative internal coordinates. This allows one to establish a relationship between the formalisms in [6] and [7]. Finally the resulting expressions for vibronic intensity are presented.

2.1. Construction of the coupling operators in absolute coordinates

The d electrons experience the attractive force of the metal nucleus and the repulsive forces of the surrounding ligands. Both metal and ligand displacements may thus give rise to vibronic coupling. It will be assumed that the coupling to the metal displacement is very strong, so that the electrons follow the motions of the metal instantaneously. Under such an *adiabatic* assumption, the radius vector of electron i, $\boldsymbol{r}_i$, is effectively centered on the metal [8]. In contrast, the radius vectors of metal and ligand L, denoted as $\boldsymbol{R}_M$ and $\boldsymbol{R}_L$ respectively, are defined with respect to a fixed coordinate origin, as depicted below.

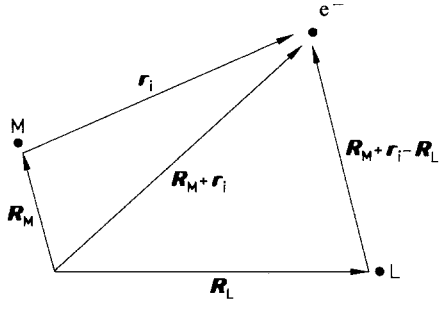

The crystal field potential for an hexacoordinated complex in the above coordinate frame is expressed in the following way:

$$\mathscr{V}(\boldsymbol{R}_M, \boldsymbol{R}_L) = \sum_{i=1}^{n} \sum_{L=1}^{6} \frac{|q_L|e^2}{|\boldsymbol{R}_M + \boldsymbol{r}_i - \boldsymbol{R}_L|}, \tag{1}$$

where $q_L e$ is the formal ligand charge.

If the metal is fixed in the origin of the coordinate frame, this expression may be converted to the usual form of the crystal field potential:

$$\mathscr{V}(0, \boldsymbol{R}_L) = \sum_{i=1}^{n} \sum_{L=1}^{6} |q_L|e^2 \sum_{l=0}^{\infty} \sum_{m=-l}^{+l} \frac{4\pi}{2l+1} \frac{r_i^l}{R_L^{l+1}} Y_m^l(i) \bar{Y}_m^l(L). \tag{2}$$

Here R_L is the metal-ligand distance and r_i represents the radial coordinate of electron i; Y_m^l is the usual spherical harmonic function [9]. The lm basis may be transformed to a $\Gamma\gamma$ basis, which is adapted to the point group symmetry of the complex:

$$\mathscr{V}(0, \boldsymbol{R}_L) = \sum_{i} \sum_{L} |q_L|e^2 \sum_{l} \sum_{\tau\Gamma\gamma} \frac{4\pi}{2l+1} \frac{r_i^l}{R_L^{l+1}} Y_{\tau\Gamma\gamma}^l(i) \bar{Y}_{\tau\Gamma\gamma}^l(L). \tag{3}$$

It should be kept in mind that this expression is only valid for $r_i < R_L$. The index τ accounts for multiple occurrence of the Γ representation in the decomposition of a given l set. The standard forms of the relevant odd $Y_{t_{1u}}^l(i)$ and $Y_{t_{2u}}^l(i)$ functions, with $l = 1, 3, 5$, are given in Table 1.

To first order, the crystal field potential may be rewritten as the sum of the static crystal field potential and a vibronic coupling term which is linear in the nuclear displacements.

$$\mathscr{V}(\boldsymbol{R}_M, \boldsymbol{R}_L) = \mathscr{V}(0, \boldsymbol{R}_L^0) + \sum_{A\lambda} \left(\frac{\partial \mathscr{V}}{\partial S_{A\lambda}}\right)_0 S_{A\lambda}. \tag{4}$$

Here $\boldsymbol{R}_L^0$ denotes the equilibrium position of ligand L. $S_{A\lambda}$ refers to a symmetry coordinate which transforms as the λ component of the A representation of O_h. Eventually an index may be added which distinguishes different coordinates of

Table 1. Standard symmetry adapted forms of the spherical harmonic functions of t_{1u} and t_{2u} symmetry[a]. Only the z components are shown

		$t_{1u}z$	$t_{2u}z$
$l=1$		Y_0^1	—
$l=3$		Y_0^3	$\frac{1}{\sqrt{2}}(Y_2^3 + Y_{-2}^3)$
$l=5$	a	Y_0^5	$\frac{1}{\sqrt{2}}(Y_2^5 + Y_{-2}^5)$
	b	$\frac{1}{\sqrt{2}}(Y_4^5 + Y_{-4}^5)$	—

[a] The multiplicity labels a and b distinguish the two t_{1u} representations contained in the $l = 5$ functions

the same symmetry. In an octahedron the odd parity coordinates, which will induce electric transition dipoles, are of t_{1u} and t_{2u} symmetry. Following the conventions of Kupka et al., the z components of these coordinates are defined as

$$\begin{aligned} S^A_{t_{1u}z} &= \tfrac{1}{2}(Z_1 + Z_2 + Z_4 + Z_5), \\ S^B_{T_{1u}z} &= \frac{1}{\sqrt{2}}(Z_3 + Z_6), \\ S^C_{t_{1u}z} &= Z_M, \\ S_{t_{2u}z} &= \tfrac{1}{2}(Z_1 - Z_2 + Z_4 - Z_5). \end{aligned} \tag{5}$$

Here, X, Y and Z refer to cartesian displacement coordinates of the nuclei in an external coordinate system, as shown in Fig. 1. The central metal ion is placed in the origin of this system. A, B and C are indices which account for the presence of three different t_{1u} coordinates. In the formalism of Kupka et al., the vibronic coupling operator in Eq. (4) is now rewritten as

$$\left(\frac{\partial \mathscr{V}}{\partial S_{\Lambda\lambda}}\right)_0 = \sum_i \sum_{l\tau} A_{l\tau\Lambda} r_i^l Y^l_{\tau\Lambda\lambda}(i). \tag{6}$$

If $S_{\Lambda\lambda}$ displaces ligands only, the coupling constants $A_{l\tau\Lambda}$ which appear in Eq. (6) may easily be derived by differentiating the crystal field potential $\mathscr{V}(0, \boldsymbol{R}_L)$ in Eq. (3). In doing so, it must be kept in mind that a $\Lambda\lambda$ type displacement will only affect the $\Gamma\gamma = \Lambda\lambda$ terms in $\mathscr{V}$. Hence

$$A_{l\tau\Lambda} = \sum_L \frac{4\pi |q_L| e^2}{2l+1} \left(\frac{\partial}{\partial S_{\Lambda\lambda}} \frac{1}{R_L^{l+1}} \bar{Y}^l_{\tau\Lambda\lambda}(L)\right)_0. \tag{7}$$

It can easily be demonstrated that this expression is indeed independent [10] of the subrepresentations λ. For the $S^C_{t_{1u}}$ coordinate, which refers to the displacement of the central metal ion, the calculation of the A constants is less obvious, since the appropriate coordinates are not contained in $\mathscr{V}(0, \boldsymbol{R}_L)$. However, from

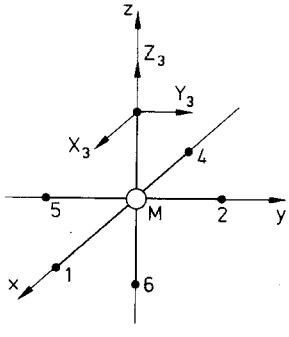

Fig 1. Coordinate system and Cartesian displacement coordinates of ligand 3

Eq. (1) the following equality may easily be shown to hold:

$$\frac{\partial \mathscr{V}(\boldsymbol{R}_M, \boldsymbol{R}_L)}{\partial X_0} = -\sum_L \frac{\partial \mathscr{V}(\boldsymbol{R}_M, \boldsymbol{R}_L)}{\partial X_L}. \tag{8}$$

This equality indicates that a displacement of the metal nucleus has the same effect on the potential as a uniform displacement of all ligands in the opposite direction. It is a direct consequence of the adiabatic coupling between the electrons and the metal displacement. Equation (8) may be rewritten as

$$\left(\frac{\partial}{\partial X_0} + \sum_L \frac{\partial}{\partial X_L}\right) \mathscr{V}(\boldsymbol{R}_M, \boldsymbol{R}_L) = 0, \tag{9}$$

and similarly for the Y and Z components.

In this way the vibronic coupling constants, associated with a moving central cation, may be related to the A constants of the peripheral modes, yielding

$$A^C_{t\tau t_{1u}} + 2A^A_{t\tau t_{1u}} + \sqrt{2}A^B_{t\tau t_{1u}} = 0. \tag{10}$$

The resulting coupling constants are collected in Table 2. It may be noted that the signs of these constants can be verified easily, using a simple pictorial representation. This is exemplified in Fig. 2, which shows a polar representation of the appropriate multipole components, in combination with the usual arrows that indicate the direction of ligand motion for positive values of S. *Whenever the ligands are moving towards the positive lobes of the multipole functions, the corresponding A constant must be positive. Otherwise it will be negative.*

In the paper by Kupka et al. the signs of the $A^B_{t\tau t_{1u}}$ parameters were misprinted. Unfortunately this error has propagated into the calculation of the $A^C_{t\tau t_{1u}}$ values giving rise to erroneous numerical results. On the other hand, it may be verified that the vibronic coupling operators of Acevedo and Flint [7, 11] coincide with the present results; however, these authors refer to internal coordinates (vide infra, Sect. 2.2), and so do not specify the $A^C_{t\tau t_{1u}}$ constants. For

Table 2. Coupling parameters $A_{t\tau A}$ for the odd parity modes in an octahedral complex[a]

	$A^A_{t\tau t_{1u}}$	$A^B_{t\tau t_{1u}}$	$A^C_{t\tau t_{1u}}$	$A_{t\tau t_{2u}}$
$l=1$	$4\sqrt{\frac{\pi}{3}}$	$-8\sqrt{\frac{\pi}{6}}$	0	0
$l=3$	$-6\sqrt{\frac{\pi}{7}}$	$-16\sqrt{\frac{\pi}{14}}$	$4\sqrt{7\pi}$	$2\sqrt{\frac{15\pi}{7}}$
$l=5$ a	$\frac{15}{2}\sqrt{\frac{\pi}{11}}$	$-24\sqrt{\frac{\pi}{22}}$	$9\sqrt{\frac{\pi}{11}}$	$-\sqrt{\frac{105\pi}{11}}$
b	$\frac{3}{2}\sqrt{\frac{35\pi}{11}}$	0	$-3\sqrt{\frac{35\pi}{11}}$	0

[a] All values must be multiplied by $|q_L|e^2/R_0^{l+2}$. The multiplicity labels a and b are defined in Table 1

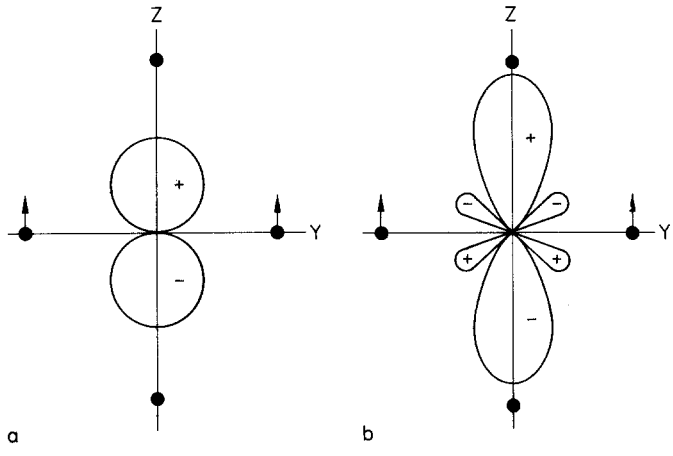

Fig. 2. Pictorial representation of the coupling constants $A^A_{1t_{1u}}$ (**a**) and $A^A_{3t_{1u}}$ (**b**). The ligands are displaced towards the positive lobe of Y^1_0, but towards the negative lobes of Y^3_0 (only the yz plane is shown). Accordingly $A^A_{1t_{1u}}$ will be positive, while $A^A_{3t_{1u}}$ is negative (see Table 2)

the moment we will pursue the absolute coordinate treatment of Kupka et al., which is more transparent as far as the translational invariance of the resulting coordinates is concerned.

The final step of their treatment involves the transformation from symmetry coordinates $S_{\Lambda\lambda}$ to normalized mass-weighted normal coordinates Q_v, which diagonalize the molecular force field. In the case of the t_{2u} representation this transformation is trivial since there is only one normal mode of t_{2u} symmetry. In contrast, the transformation from the three mass-weighted $S_{t_{1u}}$ coordinates (see Eq. (5)) to the normal coordinates of t_{1u} symmetry requires an *orthogonal* 3×3 matrix $\boldsymbol{a}$. One has

$$\begin{pmatrix} Q_{3p} \\ Q_{4p} \\ Q_{tp} \end{pmatrix} = \begin{pmatrix} a_3^A & a_3^B & a_3^C \\ a_4^A & a_4^B & a_4^C \\ a_t^A & a_t^B & a_t^C \end{pmatrix} \begin{pmatrix} \sqrt{m} & S^A_{t_{1u}p} \\ \sqrt{m} & S^B_{t_{1u}p} \\ \sqrt{M} & S^C_{t_{1u}p} \end{pmatrix},$$

$$Q_{6p} = \sqrt{m} S_{t_{2u}p}. \tag{11}$$

In Eq. (11) Q_3 and Q_4 are the usual designations for the high and low frequency t_{1u} modes, Q_t refers to the translational mode at zero frequency, Q_6 is the t_{2u} mode and M and m are the masses of the central metal and a ligand point respectively; p stands for the x, y or z components of t_{1u} and t_{2u}. The actual values of the matrix elements depend on the elastic properties of the molecule. Detailed force field calculations will be presented in Sect. 4. The vibronic coupling operator may now be rewritten as a function of the normal modes:

$$\sum_{\Lambda\lambda} \left(\frac{\partial \mathscr{V}}{\partial S_{\Lambda\lambda}} \right)_0 S_{\Lambda\lambda} = \sum_{vp} \left(\frac{\partial \mathscr{V}}{\partial Q_{vp}} \right)_0 Q_{vp}. \tag{12}$$

Combining Eqs. (6) and (11), the linear coupling terms for the t_{1u} operator

in an octahedral complex are found to be

$$\left(\frac{\partial \mathscr{V}}{\partial Q_{vp}}\right)_0 = \sum_i \sum_l \sum_\tau \left\{\frac{a_v^A A^A_{l\tau t_{1u}}}{\sqrt{m}} + \frac{a_v^B A^B_{l\tau t_{1u}}}{\sqrt{m}} + \frac{a_v^C A^C_{l\tau t_{1u}}}{\sqrt{M}}\right\} r_i^l Y^l_{\tau t_{1u} p}(i) \tag{13}$$

with $v = 3, 4$, t and $p = x, y, z$. Likewise one has for the t_{2u} mode,

$$\left(\frac{\partial \mathscr{V}}{\partial Q_{6p}}\right)_0 = \sum_i \sum_l \sum_\tau \frac{A_{l\tau t_{2u}}}{\sqrt{m}} r_i^l Y^l_{\tau t_{2u} p}(i). \tag{14}$$

For the translational motion the a coefficients are simple functions of the nuclear masses, namely

$$\begin{aligned} a_t^A &= [4m/(6m + M)]^{1/2}, \\ a_t^B &= [2m/(6m + M)]^{1/2}, \\ a_t^C &= [M/(6m + M)]^{1/2}. \end{aligned} \tag{15}$$

Inserting these values in Eq. (13) yields

$$\left(\frac{\partial \mathscr{V}}{\partial Q_{tp}}\right)_0 = \sum_i \sum_l \sum_\tau \{2A^A_{l\tau t_{1u}} + \sqrt{2}A^B_{l\tau t_{1u}} + A^C_{l\tau t_{1u}}\} \frac{r_i^l Y^l_{\tau t_{1u} p}(i)}{(6m + M)^{1/2}}. \tag{16}$$

In view of the zero condition in Eq. (10), this expression is seen to vanish, as required by the translational invariance of the vibronic coupling operator. This concludes our discussion of the coupling formalism in absolute coordinates. Subsequently we will consider the transformation to an internal coordinate system.

2.2. Construction of the coupling operators in a relative coordinate system

Since an overall translation has no vibronic effect, the previous treatment may be reformulated in a relative coordinate system of internal nuclear coordinates. Such a coordinate change will affect two important steps of the formalism, viz. the calculation of the vibronic coupling constants $A_{l\tau\Lambda}$ and the transformation of symmetry coordinates to normal coordinates. Evidently the invariance of the formalism as a whole can only be guaranteed if both steps make use of the same conventions.

Acevedo and Flint [7] base their treatment on the internal symmetry coordinates of Liehr and Ballhausen [12]. These are obtained from the absolute coordinates in Eq. (5) by relating all ligand displacements to the metal displacement rather than to the coordinate origin. The resulting internal coordinates are labeled S_3, S_4 and S_6. In the conventions of [7] the z components are given by

$$\begin{aligned} S_{3z} &= \frac{1}{\sqrt{2}}(Z_3 - Z_M + Z_6 - Z_M), \\ S_{4z} &= \tfrac{1}{2}(Z_1 - Z_M + Z_2 - Z_M + Z_4 - Z_M + Z_5 - Z_M), \\ S_{6z} &= \tfrac{1}{2}[Z_1 - Z_M - (Z_2 - Z_M) + Z_4 - Z_M - (Z_5 - Z_M)]. \end{aligned} \tag{17}$$

The relationship between internal (Eq. (17)) and external (Eq. (5)) symmetry coordinates reads

$$\begin{aligned} S_{3p} &= S^B_{t_{1u}p} - \sqrt{2}S^C_{t_{1u}p}, \\ S_{4p} &= S^A_{t_{1u}p} - 2S^C_{t_{1u}p}, \\ S_{6p} &= S_{t_{2u}p}. \end{aligned} \tag{18}$$

In view of adiabaticity constraint in Eq. (9), the following identity may be shown to hold:

$$\begin{aligned} \frac{\partial \mathscr{V}}{\partial(Z_K - Z_M)} &= \sum_L \frac{\partial Z_L}{\partial(Z_K - Z_M)} \frac{\partial \mathscr{V}}{\partial Z_L} + \frac{\partial Z_M}{\partial(Z_K - Z_M)} \frac{\partial \mathscr{V}}{\partial Z_0} \\ &= \sum_L \frac{\partial Z_L}{\partial(Z_K - Z_M)} \frac{\partial \mathscr{V}}{\partial Z_L} - \sum_L \frac{\partial Z_M}{\partial(Z_K - Z_M)} \frac{\partial \mathscr{V}}{\partial Z_L} \\ &= \sum_L \frac{\partial(Z_L - Z_M)}{\partial(Z_K - Z_M)} \frac{\partial \mathscr{V}}{\partial Z_L} \\ &= \frac{\partial \mathscr{V}}{\partial Z_K}. \end{aligned} \tag{19}$$

Because of this identity the coupling constants for the internal coordinates, S_3, S_4 and S_6, will simply coincide with the constants for the corresponding absolute ligand displacements, $S^B_{t_{1u}}$, $S^A_{t_{1u}}$ and $S_{t_{2u}}$ respectively. Hence one has that

$$\begin{aligned} \left(\frac{\partial \mathscr{V}}{\partial S_{3p}}\right)_0 &= \sum_i \sum_l \sum_\tau A^B_{l\tau t_{1u}} r_i^l Y^l_{\tau t_{1u}p}(i), \\ \left(\frac{\partial \mathscr{V}}{\partial S_{4p}}\right)_0 &= \sum_i \sum_l \sum_\tau A^A_{l\tau t_{1u}} r_i^l Y^l_{\tau t_{1u}p}(i), \\ \left(\frac{\partial \mathscr{V}}{\partial S_{6p}}\right)_0 &= \sum_i \sum_l \sum_\tau A_{l\tau t_{2u}} r_i^l Y^l_{\tau t_{1u}p}(i). \end{aligned} \tag{20}$$

As before, these terms must now be recombined to yield the vibronic coupling constants for the normalized mass-weighted normal coordinates Q_ν, which incorporate the elastic properties of the molecular force field. The relevant transformation matrix is usually denoted by the $\boldsymbol{L}$ matrix, and is defined as

$$\begin{aligned} \begin{pmatrix} S_{3p} \\ S_{4p} \end{pmatrix} &= \begin{pmatrix} L_{33} & L_{34} \\ L_{43} & L_{44} \end{pmatrix} \begin{pmatrix} Q_{3p} \\ Q_{4p} \end{pmatrix}, \\ S_{6p} &= L_{66} Q_{6p}. \end{aligned} \tag{21}$$

Unlike the $\boldsymbol{a}$ matrix in Eq. (11), $\boldsymbol{L}$ is non-orthonormal. The linear coupling terms

thus become

$$\left(\frac{\partial \mathscr{V}}{\partial Q_{3p}}\right)_0 = L_{33}\left(\frac{\partial \mathscr{V}}{\partial S_{3p}}\right)_0 + L_{43}\left(\frac{\partial \mathscr{V}}{\partial S_{4p}}\right)_0,$$
$$\left(\frac{\partial \mathscr{V}}{\partial Q_{4p}}\right)_0 = L_{34}\left(\frac{\partial \mathscr{V}}{\partial S_{3p}}\right)_0 + L_{44}\left(\frac{\partial \mathscr{V}}{\partial S_{4p}}\right)_0, \tag{22}$$
$$\left(\frac{\partial \mathscr{V}}{\partial Q_{6p}}\right)_0 = L_{66}\left(\frac{\partial \mathscr{V}}{\partial S_{6p}}\right)_0.$$

In order to establish the strict equivalence between these results and the outcome of the previous treatment, we first derive the conversion formulae for the elements of $\boldsymbol{L}$ and $\boldsymbol{a}$. This is done by combining Eqs. (11), (15), (18) and (21). One readily obtains (with $v = 3, 4$)

$$L_{3v} = \frac{a_v^B}{\sqrt{m}} - \frac{\sqrt{2}a_v^C}{\sqrt{M}},$$
$$L_{4v} = \frac{a_v^A}{\sqrt{m}} - \frac{2a_v^C}{\sqrt{M}}, \tag{23}$$
$$L_{66} = \frac{1}{\sqrt{m}}.$$

Substitution of the coefficients and derivatives into the right hand side of Eq. (22) yields

$$\left(\frac{\partial \mathscr{V}}{\partial Q_{vp}}\right)_0 = \sum_i \sum_l \sum_\tau \left\{A^A_{l\tau t_{1u}}\left(\frac{a_v^A}{\sqrt{m}} - \frac{2a_v^C}{\sqrt{M}}\right) + A^B_{l\tau t_{1u}}\left(\frac{a_v^B}{\sqrt{m}} - \frac{\sqrt{2}a_v^C}{\sqrt{M}}\right)\right\} r_i^l Y^l_{\tau t_{1u}p}(i),$$
$$\left(\frac{\partial \mathscr{V}}{\partial Q_{6p}}\right)_0 = \sum_i \sum_l \sum_\tau \frac{A_{l\tau t_{2u}}}{\sqrt{m}} r_i^l Y^l_{\tau t_{2u}p}(i) \qquad (\text{with } v = 3, 4;\ p = x, y, z). \tag{24}$$

Furthermore, using Eq. (10), the expressions for the t_{1u} operators in Eq. (24) may be rearranged to yield

$$\left(\frac{\partial \mathscr{V}}{\partial Q_{vp}}\right)_0 = \sum_i \sum_l \sum_\tau \left\{\frac{a_v^A A^A_{l\tau t_{1u}}}{\sqrt{m}} + \frac{a_v^B A^B_{l\tau t_{1u}}}{\sqrt{m}} + \frac{a_v^C A^C_{l\tau t_{1u}}}{\sqrt{M}}\right\} r_i^l Y^l_{\tau t_{1u}p}(i). \tag{13bis}$$

This is precisely the result obtained by Kupka et al. A similar correspondence is noted for the t_{2u} operator in Eqs. (14) and (24). In this way the strict equivalence of the formalisms in [6] and [7] is established.

We recall that this result only holds if *identical* internal symmetry coordinates are used in the calculation of the A constants (Eq. (20)) and in the force field calculation of the normal modes (Eq. (21)). This point has been overlooked in [7]. In this paper the vibronic coupling constants were calculated using the S_3, S_4 and S_6 coordinates of Eq. (17), but the conversion to normal modes was based on a different set of internal symmetry coordinates, which is of standard use in

typical Wilsonian force field studies [13]. In such studies the internal bending coordinates are expressed by means of bond angle changes and are normalized accordingly. As an example the t_{2u} bending coordinate, S_6, is usually defined as

$$\frac{R_0}{\sqrt{8}}(-\Delta\alpha_{13}+\Delta\alpha_{16}+\Delta\alpha_{23}-\Delta\alpha_{26}-\Delta\alpha_{34}+\Delta\alpha_{46}+\Delta\alpha_{35}-\Delta\alpha_{56}), \tag{25}$$

where R_0 is the complex radius at equilibrium. The bond angle changes $\Delta\alpha_{ij}$ may be replaced by cartesian displacement coordinates [14] in the following way:

$$\begin{aligned} R_0\,\Delta\alpha_{13} &= -Z_1+Z_0-X_3+X_0, \\ R_0\,\Delta\alpha_{23} &= -Z_2+Z_0-Y_3+Y_0, \\ &\text{etc.} \end{aligned} \tag{26}$$

Upon substitution the bending coordinate in Eq. (25) is seen to correspond to $\sqrt{2}S_{6z}$; a similar $\sqrt{2}$ factor is needed for the S_4 bending coordinate. Hence the corresponding L elements of typical force field studies must be divided by $\sqrt{2}$ (not to mention possible phase changes) before they can be introduced into the present formalism.

We note that this fact was recognized in the study of Liehr and Ballhausen [12] on the Jahn–Teller instability of E_g electronic states; however in [7] the $\sqrt{2}$ factors were omitted, leading to incorrect numerical results. In order to avoid further confusion, the subsequent treatment, including the force field calculations in Sect. 4, will be formulated entirely in the absolute coordinate system of Kupka et al.

2.3. General expressions for the intensities of vibronic side bands

In vibronic intensity calculations for d–d transitions, the vibronic coupling operators $(\partial\mathscr{V}/\partial Q_{vp})_0$ are combined with the transition dipole operator to yield the so-called forced dipole transition moments. These moments can be constructed in two different ways, depending on the nature of the intermediate states that are being invoked. Ballhausen and Liehr [1] proposed to use the $d^{n-1}p$ states that originate from exciting a single d electron into the empty p shell. Koide and Pryce [2] on the other hand preferred to sum over all allowed transitions, thereby adopting the closure approximation. The subsequent discussion will be focused entirely on the latter formalism. Here we repeat the most relevant expressions of the Koide and Pryce method. For a more detailed treatment, the reader is referred to the original papers [1, 2, 15].

In the closure approximation the transition operator is composed of the product of the dipole operator and the vibronic coupling operators specified previously. As an example, for a y polarized transition induced by a Q_{vp} vibration, the electronic transition operator corresponds to $\sum_i ey(i)\cdot(\partial\mathscr{V}/\partial Q_{vp})_0$. This moment must be weighted by a $2/\Delta E$ parameter, where ΔE represents the average energy gap between the d^n states and the ungerade intermediate states. As a result,

the effective electronic transition moment for a $\Gamma_0\gamma_0 \rightarrow \Gamma\gamma$ transition is given by

$$F_{y\cdot vp}^{\Gamma_0\gamma_0\rightarrow\Gamma\gamma} = \frac{2}{\Delta E}\langle d^n\Gamma_0\gamma_0 \left| \sum_i ey(i)\cdot(\partial\mathscr{V}/\partial Q_{vp})_0 \right| d^n\Gamma\gamma\rangle. \tag{27}$$

If the molecular force field is not seriously affected by the electronic excitation, the vibronic intensity will be concentrated in false origins, involving single quanta of the allowing odd modes. The relative intensities of these vibronic side bands are proportional to the electronic transition element and inversely proportional to the vibrational angular frequency of the allowing mode [16] symbolized as ω_v.

$$I_v \propto \frac{1}{\omega_v}\sum_{\gamma_0\gamma p}\left|F_{y\cdot vp}^{\Gamma_0\gamma_0\rightarrow\Gamma\gamma}\right|^2 \quad \text{with } v = 3,\ 4,\ 6. \tag{28}$$

In Sect. 4, this expression will be used to compare the intensities of the three vibronic satellites of the $^4A_{2g} \rightarrow {}^2E_g$ transition in hexacoordinated d^3 complexes.

3. Emission spectra of d^3 complexes

Octahedral d^3 complexes have a $^4A_{2g}$ ground state and a series of low lying doublet states, labeled as ^2E_g, $^2T_{1g}$, $^2T_{2g}$. All these states are based on a common half-filled shell $(t_{2g})^3$ configuration. As a result they will be characterized by nearly identical force fields [17, 18], a prerequisite for the application of the Koide and Pryce intensity formalism. The sharp line phosphorescence spectra of the hexahalide complexes of the $3d^3$ ions, Cr^{3+} and Mn^{4+}, offer unrivalled examples of vibronic coupling in d–d transitions [19]. Indeed, the most prominent features of the low temperature spectra arise from a weak magnetic dipole allowed pure electronic origin and three strong vibronic origins, corresponding to the ν_3, ν_4 and ν_6 odd parity modes. These features are virtually unaffected by changes in the lattice environment. An isolated molecule analysis, assuming the tight binding approximation thus appears to be reasonable.

Specifically for the lowest spin-forbidden transition of $^4A_{2g} \leftrightarrow {}^2E_g$ character, the bending modes, ν_4 and ν_6, seem to be much more effective in promoting intensity than the stretching mode ν_3; this is illustrated in Table 3 [20–25]. It is

Table 3. Relative intensities for the vibronic side bands in d^3 complexes

Compound	Transition	Relative intensities[a]	References
		ν_6 : ν_4 : ν_3	
K_2NaAlF_6:CrF_6^{3-}	$^4A_{2g} \leftarrow {}^2E_g$	vvs: vs : s	[20, 21]
$Cs_2NaInCl_6$:$CrCl_6^{3-}$	$^4A_{2g} \rightarrow {}^2E_g$	vvs: vvs: s	[22]
Cs_2MnF_6	$^4A_{2g} \leftarrow {}^2E_g$	10 : 7.6 : 1	[23]
		4.5 : 4 : 1	[7, 24]
Cs_2TeCl_6:$ReCl_6^{2-}$	$\Gamma_8(^4A_{2g}) \leftarrow \Gamma_7(^2T_{2g})$	0.5 : 1.8 : 1	[6, 25]

[a] Most spectra were taken at 5 K; vvs = very very strong, vs = very strong, s = strong

noteworthy that in complexes with polyatomic ligands the same type of selectivity is observed. As an example, in the luminescence spectra of $Cr(NH_3)_6(ClO_4)_3$ the vibronic origins involving the N–Cr–N and also the Cr–N–H bending modes are an order of magnitude stronger than the Cr–N stretching mode [26, 27].

The other transitions of the doublet region do not seem to exhibit the same weakness of the ν_3 false origin. This is illustrated by the $^4A_{2g} \leftarrow {}^2T_{1g}$ excitation spectrum [19] of MnF_6^{2-} in Cs_2SiF_6. More detailed examples of the same trend are present in the spin-forbidden spectra [28, 29] of $4d^3$ hexahalides of Mo^{3+} and Tc^{4+}. In general these spectra are more intense and have a richer vibronic structure, as a result of increased spin-orbit coupling. A case in point is the luminescence spectrum of $MoCl_6^{3-}$ in cubic elpasolite crystals [28]. The near-infrared luminescence band, of $\Gamma_8(^4A_{2g}) \leftarrow \Gamma_8(^2E_g)$ signature, shows the characteristic preference for the bending modes: the ν_6 line is extremely strong, the ν_4 line is of medium intensity, while the ν_3 line is at least one order of magnitude less intense. In contrast, in the visible luminescence band, attributed to the $\Gamma_8(^4A_{2g}) \leftarrow \Gamma_8(^2T_{2g})$ transition, the ν_3 stretching mode appears to be the strongest promoting mode. Similar observations have been made for the isoelectronic $TcCl_6^{2-}$ and $TcBr_6^{2-}$ ions in various cubic lattices [29]. The loss of selectivity is even more pronounced in the spectra [6, 30] of the $5d^3$ hexahalides of Re^{4+}. This is illustrated in Table 3 for the $\Gamma_8(^4A_{2g}) \leftarrow \Gamma_7(^2T_{2g})$ transition of $ReCl_6^{2-}$ doped in Cs_2TeCl_6.

It is well established that all these spin-forbidden bands draw their intensity from the nearby $^4A_{2g} \leftarrow {}^4T_{2g}(t_{2g}^2 e_g)$ and $^4A_{2g} \leftarrow {}^4T_{1g}(t_{2g}^2 e_g)$ spin-allowed transitions via spin-orbit coupling. In this respect the ^2E_g state is unique, in that it has no spin-orbit interaction element with the $^4T_{1g}$ state, and therefore obtains its intensity almost exclusively from the $^4A_{2g} \rightarrow {}^4T_{2g}$ transition [31]. This is confirmed by complete ligand field calculations [32] for MnF_6^{2-} and $MoCl_6^{3-}$, using values of 400 cm^{-1} and 600 cm^{-1} respectively for the spin-orbit parameter ζ.

Spin-orbit coupling thus provides a selective mechanism which connects the vibronic intensity distribution in the $^4A_{2g} \leftarrow {}^2E_g$ emission to the $^4A_{2g} \leftarrow {}^4T_{2g}$ transition moment. Consequently, the weak activity of the ν_3 mode in the doublet emission implies a preferential coupling to the bending modes in the $^4A_{2g} \leftarrow {}^4T_{2g}$ transition. In the favorable case of $CrCl_6^{3-}$ in elpasolite lattices, this has been verified by direct measurement of the vibronic origins in the broadband fluorescence spectrum from the $^4T_{2g}$ state [33]. The corresponding vibronic assignments have recently been confirmed by Güdel and coworkers [34], using magnetic circularly polarized luminescence spectroscopy. Accordingly, in the subsequent calculations of relative vibronic intensities in the ^2E_g emission of Cr^{3+}, Mn^{4+} and Mo^{3+} complexes the electronic part of the transition moment will be related to the first spin-allowed transition.

In contrast, the other transitions of the doublet region mix in via spin-orbit coupling with both spin-allowed transitions. Their intensity distribution thus cannot be attributed to one single quartet band. So far there have been no attempts to deconvolute the coupling patterns of the two quartet-quartet transitions. However, from the observed loss of selectivity, it seems clear that the ν_3 stretching mode acquires a strong activity in the second spin-allowed transition.

4. Force field calculations

In order to calculate the transition moment integrals for the ν_3 and ν_4 origins, one must determine the composition of the two t_{1u} coordinates. In principle this composition may vary from the ground to the excited state, giving rise to a Dushinski effect in the t_{1u} coordinates. However in the case of the $^4A_{2g} \leftarrow {}^2E_g$ emission the force fields of initial and final states nearly coincide. As a result the normal mode analysis can be restricted to the $^4A_{2g}$ ground state.

In the literature different molecular force fields for octahedral hexahalogen molecules have been studied [13, 35]. In this section we compare the results, paying special attention to the composition of the t_{1u} modes. As a basis for comparison we have used a set of recent spectral data, including some Tc^{4+} and Re^{4+} examples [25, 29, 30, 36]. The observed frequencies are listed in Table 4. In all cases, all six fundamentals could be determined from Raman (ν_1, ν_2, ν_5), infrared (ν_3, ν_4) or emission ($\nu_1 - \nu_4$, ν_6) spectroscopy.

The normal modes of t_{1u} symmetry are obtained by diagonalizing the force field over the three mass-weighted Cartesian displacement coordinates: $\sqrt{m}S^A_{t_{1u}p}$, $\sqrt{m}S^B_{t_{1u}p}$, $\sqrt{M}S^C_{t_{1u}p}$. Since the t_{1u} interaction matrix is independent of p, the component label will be omitted from the further treatment. In the Cartesian space the t_{1u} modes may be written in a vectorial form as $(a^A_\nu, a^B_\nu, a^C_\nu)$, where the a coefficients specify the directional cosines as defined in Eq. (11). The t_{1u} interaction matrix has one zero eigenvalue, which corresponds to the translational mode: (a^A_t, a^B_t, a^C_t). This mode is normal to the plane of the two internal modes Q_3 and Q_4; it is illustrated in Fig. 3 for the MnF_6^{2-} ion. Following Koide and Pryce [2], it is convenient to define this plane of internal modes by two

Table 4. Observed vibrational frequencies (in cm^{-1}) for hexafluoride and hexachloride d^3 complexes[a]. The values in parentheses are calculated frequencies based on the Urey–Bradley force field of Table 6

	ν_1	ν_2	ν_3	ν_4	ν_5	ν_6	References
$K_2NaGaF_6:CrF_6^{3-}$	575	480	575	330	284	200	[21]
	(574)	(447)	(592)	(305)	(307)	(202)	
Cs_2MnF_6	592	508	616	332	308	228	[24]
	(592)	(484)	(628)	(310)	(327)	(227)	
Cs_2ReF_6	611	530	535	248	233	180	[30]
	(600)	(497)	(572)	(225)	(257)	(155)	
$Cs_2NaInCl_6:CrCl_6^{3-}$	298	240	324	187	139	120	[33, 34]
	(299)	(223)	(329)	(171)	(162)	(109)	
$Cs_2NaScCl_6:MoCl_6^{3-}$	314	270	298	141	145	118	[26]
	(310)	(244)	(314)	(125)	(159)	(117)	
$Cs_2TeCl_6:TcCl_6^{2-}$	333	265	335	178	177	133	[29]
	(332)	(259)	(338)	(172)	(184)	(127)	
K_2ReCl_6	359	302	315	166	173	129	[25, 36]
	(352)	(277)	(338)	(154)	(183)	(124)	

[a] Most data were obtained from the $^4A_{2g} \leftarrow {}^2E_g$ emission spectra at low temperature

orthogonal unit vectors $|\sigma_1\rangle$ and $|\sigma_2\rangle$, where the components of these vectors are

$$|\sigma_1\rangle = \left\{0, \left(\frac{M}{M+2m}\right)^{1/2}, -\left(\frac{2m}{M+2m}\right)^{1/2}\right\},$$

$$|\sigma_2\rangle = \left\{\left(\frac{M+2m}{M+6m}\right)^{1/2}, -\left(\frac{8m^2}{(M+2m)(M+6m)}\right)^{1/2}, -\left(\frac{4mM}{(M+2m)(M+6m)}\right)^{1/2}\right\}. \tag{29}$$

Clearly these components are chosen in such a way that $|\sigma_1\rangle$ corresponds to the mass-weighted internal stretching coordinate S_3, given in Eq. (18). However this does not imply that $|\sigma_2\rangle$ is oriented along the bending coordinate S_4 since the two internal symmetry coordinates are not orthogonal.

An alternative coordinate set, for which collinearity of one of the unit vectors with S_4 is realized, is given in Eq. (30)

$$|\sigma_1'\rangle = \left\{-\left(\frac{8m^2}{(M+4m)(M+6m)}\right)^{1/2}, \left(\frac{M+4m}{M+6m}\right)^{1/2}, -\left(\frac{2mM}{(M+4m)(M+6m)}\right)^{1/2}\right\},$$

$$|\sigma_2'\rangle = \left\{\left(\frac{M}{M+4m}\right)^{1/2}, 0, -\left(\frac{4m}{M+4m}\right)^{1/2}\right\}. \tag{30}$$

Here $|\sigma_2'\rangle$ corresponds to the mass-weighted S_4 coordinate. As indicated in Fig. 3, the primed set is rotated with respect to the unprimed one over an angle α, which only depends on the ratio of metal and ligand mass. One has

$$\tan\alpha = \frac{\langle\sigma_2|\sigma_1'\rangle}{\langle\sigma_1|\sigma_1'\rangle} = -\left(\frac{8m^2}{M(M+6m)}\right)^{1/2}. \tag{31}$$

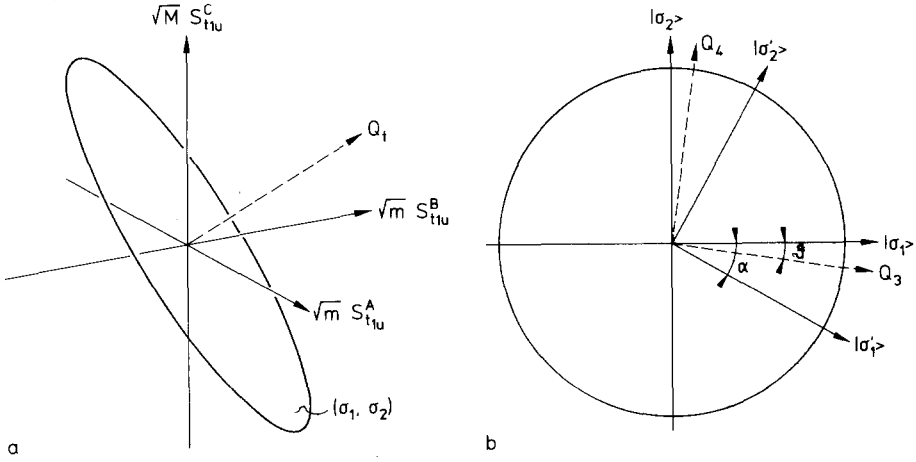

Fig. 3. a Shows the space of the three mass-weighted t_{1u} displacement coordinates. Q_t indicates the translational mode for the case of MnF_6^{2-}. The great circle (σ_1, σ_2) which is normal to Q_t, contains the two internal modes. It is shown in more detail in **b**. The two possible sets of unit vectors (σ_1, σ_2) and (σ_1', σ_2') are defined in Eqs. (29) and (30). The rotational angle α between the two sets is $-29°$. Also indicated are the Q_3 and Q_4 normal modes which result from a Urey–Bradley force field calculation for MnF_6^{2-}. The angle θ between Q_3 and σ_1 is $-7°$ (see Table 5)

Table 5. Angular parameters, describing the composition of the t_{1u} coordinates[a]

Complex	α	θ(UBFF)	θ_A(GHFF)	θ_B(GHFF)	θ_0
CrF_6^{3-}	−30	−8	−11	−49	−67
MnF_6^{2-}	−29	−7	−20	−38	−67
ReF_6^{2-}	−13	−8	+28	−53	−64
$CrCl_6^{3-}$	−41	−8	−15	−66	−71
$MoCl_6^{3-}$	−30	−15	+4	−76	−67
$TcCl_6^{2-}$	−30	−11	−23	−37	−67
$ReCl_6^{2-}$	−20	−13	−4	−36	−65

[a] All angles are given in degrees. The angle α corresponds to the difference between the (σ_1, σ_2) and (σ_1', σ_2') coordinate frames. The angles θ describe the rotation of the (Q_3, Q_4) normal modes with respect to the (σ_1, σ_2) reference frame, as defined in Eq. (32), for various force fields. The angle θ_0 describes the normal mode with zero octupole character as defined in Eq. (39)

Values for α are given in the first column of Table 5. Similarly, the composition of the actual normal modes Q_3 and Q_4 can be described by an angle θ, corresponding to a rotation of the (σ_1, σ_2) reference frame:

$$\begin{pmatrix} Q_3 \\ Q_4 \end{pmatrix} = \begin{pmatrix} \cos\theta & \sin\theta \\ -\sin\theta & \cos\theta \end{pmatrix} \begin{pmatrix} |\sigma_1\rangle \\ |\sigma_2\rangle \end{pmatrix} \quad \text{with } \tan\theta = \frac{\langle\sigma_2|Q_3\rangle}{\langle\sigma_1|Q_3\rangle}. \tag{32}$$

Hence one single angular parameter is sufficient to express the composition of the t_{1u} modes. In the following we will investigate how this parameter varies with the force field. The discussion will be centered on two representative force fields: the Urey–Bradley force field (UBFF), and the general harmonic force field (GHFF).

4.1. The UBFF

The Urey–Bradley potential for an octahedral complex [35] requires only four force constants: K, H, F and F'. K is the force constant for stretching along a bond, H for an angle deformation, F and F' for the repulsion between neighbouring ligands. The value of F' is usually much smaller than F and is sometimes taken as $-(1/10)F$.

The UBFF parametrization scheme is summarized in Eqs. (33) and (34). As usual the eigenvalues of the force field calculations are denoted as $\lambda = 4\pi^2 c^2 \nu^2$, where ν is the frequency in cm^{-1}.

$$\begin{aligned} m\lambda_1 &= K + 4F, \\ m\lambda_2 &= K + F + 3F', \\ m\lambda_5 &= 2(2H + F - F'), \\ m\lambda_6 &= 2H + F + F'. \end{aligned} \tag{33}$$

The λ_3 and λ_4 eigenvalues must be determined by diagonalizing the t_{1u} interaction matrix in Eq. (34)

	$\sqrt{m}S^A$	$\sqrt{m}S^B$	$\sqrt{M}S^C$
$\sqrt{m}S^A$	$\frac{1}{m}(2H+F-3F')$	$-\frac{\sqrt{2}}{m}(F+F')$	$\frac{4}{\sqrt{mM}}(2F'-H)$
$\sqrt{m}S^B$	$-\frac{\sqrt{2}}{m}(F+F')$	$\frac{1}{m}(K+2F+2F')$	$-\frac{\sqrt{2}}{\sqrt{mM}}K$
$\sqrt{M}S^C$	$\frac{4}{\sqrt{mM}}(2F'-H)$	$-\frac{\sqrt{2}}{\sqrt{mM}}K$	$\frac{2}{M}(K+4H-8F')$

(34)

Optimal fits for the four constants were obtained by a simplex method. The resulting parameters are listed in Table 6, and calculated frequencies in Table 4. Note that, in spite of the simplicity of the force field, there is a fair agreement between observed and calculated values. Furthermore, the F'/F ratio is indeed found to be small, and mostly negative. The angular parameter θ, describing the composition of the t_{1u} modes, is given in the second column of Table 5. Quite remarkably, θ is nearly constant for all complexes considered, with $\alpha < \theta < 0$. This means that the actual normal modes (Q_3, Q_4) are rotated with respect to the (σ_1, σ_2) reference frame in the direction of the (σ_1', σ_2') frame. In this way the UBFF optimizes the overlap between the normal t_{1u} modes and the internal t_{1u} symmetry coordinates. Similar results may be obtained for the modified UBFF, for the Orbital Valence Force Field (OVFF) of Heath and Linnet, and for the corresponding modified OVFF [35]. Clearly in all these cases, the solution of the t_{1u} multiplicity problem is based on a maximal deconvolution of bending and stretching interactions.

Table 6. Calculated Urey–Bradley force constants (in N m^{-1}) for the complexes in Table 4

Complex	K	F	H	F'
CrF_6^{3-}	189	45	2	−3
MnF_6^{2-}	222	42	8	−1[a]
ReF_6^{2-}	254	37	−3	−5
$CrCl_6^{3-}$	82	26	0	−1
$MoCl_6^{3-}$	95	26	0.5	1
$TcCl_6^{2-}$	113	29	3	−1
$ReCl_6^{2-}$	133	31	1	−1

[a] These parameter values for MnF_6^{2-} give a slightly better fit than the results in [7]

4.2. The GHFF

The GHFF method takes into account all possible harmonic interactions between bond stretchings and angle deformations. GHFF expressions for octahedral molecules were developed by Pistorius [37] and the results may be summarized as follows:

$$
\begin{aligned}
m\lambda_1 &= f_r + 4f_{rr} + f_{rr'},\\
m\lambda_2 &= f_r - 2f_{rr} + f_{rr'},\\
m\lambda_3 m\lambda_4 &= \frac{M+6m}{M}[2(f_r - f_{rr'})(f_\alpha - f_{\alpha\alpha'''} + 2(f_{\alpha\alpha} - f_{\alpha\alpha''})) - 8(f_{r\alpha} - f_{r\alpha''})^2],\\
m\lambda_3 + m\lambda_4 &= \frac{M+2m}{M}(f_r - f_{rr'}) - \frac{16m}{M}(f_{r\alpha} - f_{r\alpha''})\\
&\quad + \frac{2M+8m}{M}(f_\alpha - f_{\alpha\alpha'''} + 2(f_{\alpha\alpha} - f_{\alpha\alpha''})),\\
m\lambda_5 &= 4(f_\alpha - f_{\alpha\alpha'''} - 2(f_{\alpha\alpha'} - f_{\alpha\alpha'''})),\\
m\lambda_6 &= 2(f_\alpha - f_{\alpha\alpha'''} - 2(f_{\alpha\alpha} - f_{\alpha\alpha''})).
\end{aligned}
\tag{35}
$$

Here the f force constants follow the definitions of [37]. If $f_{rr'}$ is neglected, there are six independent combinations of force constants to be determined from an equal number of frequency expressions. However since one of these expressions contains a quadratic term in $f_{r\alpha} - f_{r\alpha''}$, two sets of solutions will be obtained; these are listed in Table 7. The t_{1u} normal modes can now be obtained by inserting the λ_3 and λ_4 eigenvalues in the t_{1u} interaction matrix, given below.

	$\sqrt{m}S^A_{t_{1u}}$	$\sqrt{m}S^B_{t_{1u}}$	$\sqrt{M}S^C_{t_{1u}}$
$\sqrt{m}S^A_{t_{1u}}$	$\frac{2}{m}(f_\alpha - f_{\alpha\alpha'''} + 2f_{\alpha\alpha} - 2f_{\alpha\alpha''})$	$-\frac{2\sqrt{2}}{m}(f_{r\alpha} - f_{r\alpha''})$	$\frac{4}{\sqrt{mM}}(-f_\alpha + f_{\alpha\alpha'''} - 2f_{\alpha\alpha} + 2f_{\alpha\alpha''} + f_{r\alpha} - f_{r\alpha''})$
$\sqrt{m}S^B_{t_{1u}}$		$\frac{1}{m}(f_r - f_{rr'})$	$\frac{\sqrt{2}}{\sqrt{mM}}(-f_r + f_{rr'} + 4f_{r\alpha} - 4f_{r\alpha''})$
$\sqrt{M}S^C_{t_{1u}}$			$\frac{2}{M}(f_r - f_{rr'} - 8f_{r\alpha} + 8f_{r\alpha''} + 4f_\alpha - 4f_{\alpha\alpha'''} + 8f_{\alpha\alpha} - 8f_{\alpha\alpha''})$

(36)

The θ angles are listed in Table 5. The column, marked θ_A, corresponds to the set with smaller $f_{r\alpha} - f_{r\alpha''}$, while the θ_B column refers to solutions with larger $f_{r\alpha} - f_{r\alpha''}$. For most complexes the θ_A values show reasonable agreement with the

Table 7. Calculated GHFF parameters[a] (in $N\,m^{-1}$) for the complexes in Table 4

A solution[b]	f_r	$f_{rr'}$	$f_{r\alpha}-f_{r\alpha''}$	$f_{\alpha}-f_{\alpha\alpha'''}$	$f_{\alpha\alpha}-f_{\alpha\alpha''}$	$f_{\alpha\alpha'}-f_{\alpha\alpha'''}$
CrF_6^{3-}	295	19	23	23	0.2	0.1
MnF_6^{2-}	323	17	4	36	4	5
ReF_6^{2-}	349	17	−62	41	12	13
$CrCl_6^{3-}$	142	11	17	18	1	4
$MoCl_6^{3-}$	170	9	−31	−18	−16	−15
$TcCl_6^{2-}$	175	14	22	22	2	3
$ReCl_6^{2-}$	217	13	4	5	−6	−5
B solutions[c]						
CrF_6^{3-}	295	19	65	48	13	13
MnF_6^{2-}	323	17	56	47	9	10
ReF_6^{2-}	349	17	113	92	37	38
$CrCl_6^{3-}$	142	11	35	79	32	34
$MoCl_6^{3-}$	170	9	82	73	29	31
$TcCl_6^{2-}$	175	14	30	27	4	5
$ReCl_6^{2-}$	217	13	43	22	3	3

[a] The parameter $f_{rr'}$ is put equal to zero
[b] The A solution corresponds to the smaller value of $f_{r\alpha}-f_{r\alpha''}$, and is generally considered to be the "physical one"
[c] The B solution corresponds to the larger value of $f_{r\alpha}-f_{r\alpha''}$

UBFF results. Hence for the A set, bending and stretching modes remain approximately separated [38]. This is of course in line with the small values for the $f_{r\alpha}-f_{r\alpha''}$ bending-stretching interaction constants. In contrast the B set is quite different, with $\theta_B < \alpha$. Hence for this solution the normal modes are rotated beyond the (σ_1', σ_2') coordinate system. Such a solution of the t_{1u} multiplicity problem can no longer be characterized as a separation of bending and stretching modes. It rather corresponds to a separation of electric multipoles, as will be discussed in the next section.

In order to determine which of the two solutions is the "physical" one, additional information is required. A convenient criterion involves comparison of the vibrational amplitudes calculated for both sets with electron diffraction results [39]. This has yielded conclusive evidence to reject the θ_B solutions in the case of volatile compounds [40, 41] such as WF_6 and UF_6. To our knowledge no similar comparison has been carried out for the d^3 complexes under study. Nonetheless it seems extremely unlikely that the elastic properties of these complexes should show a different pattern.

In conclusion, force field calculations suggest that the composition of the t_{1u} modes is restricted to a small angular interval, preferably with $\alpha < \theta < 0$.

5. Intensity calculations

In this section we apply the vibronic intensity formalism to the ${}^4A_{2g} \leftarrow {}^2E_g$ emission lines in d^3 complexes. Our main concern is to explain how vibronic selectivity can arise. In principle different selection rules are possible, depending

on the relative strength of the coupling parameters. Before examining these in detail, attention is given to some general symmetry aspects.

5.1. *Symmetry analysis*

As we have shown in Sect. 3, for complexes of moderate spin-orbit coupling strength the electronic part of the transition integrals reduces to a matrix element over the ${}^4A_{2g} \leftarrow {}^4T_{2g}$ transition. The required elements can easily be calculated with tensorial methods, and the results are listed in Table 8. Clearly in the d-only approximation, the allowed tensorial ranks of operators connecting two d^3 states are limited to 0, 2 and 4. A further restriction arises from the finite group selection rule, which states that the total transition operator must transform according to the $A_{2g} \times T_{2g} = T_{1g}$ representation of O_h. The octahedral symmetry

Table 8. Electronic wave functions and matrix elements of the ${}^4A_{2g} \leftrightarrow {}^4T_{2g}$ transition in y polarization

Wavefunctions[a]			
$\lvert {}^4A_{2g} \rangle = -\lvert (d_{yz})(d_{xz})(d_{xy}) \rvert$			
$\lvert {}^4T_{2g}x \rangle = \left\lvert \left(\frac{\sqrt{3}}{2} d_{z^2} + \frac{1}{2} d_{x^2-y^2} \right)(d_{xz})(d_{xy}) \right\rvert$			
$\lvert {}^4T_{2g}y \rangle = \left\lvert \left(\frac{\sqrt{3}}{2} d_{z^2} - \frac{1}{2} d_{x^2-y^2} \right)(d_{yz})(d_{xy}) \right\rvert$			
$\lvert {}^4T_{2g}z \rangle = -\lvert (d_{x^2-y^2})(d_{yz})(d_{xz}) \rvert$			
Matrix elements[b]: $\langle {}^4A_{2g} \lvert \sum_i ey(i) \cdot \sum_j r_j^l Y_{\tau\Gamma p}^l \rvert {}^4T_{2g} q \rangle$			
	t_{1u}	t_{1u}	t_{2u}
	$p = z,\ q = x$	$p = x,\ q = z$	$p = z,\ q = x$ $p = x,\ q = z$
$l = 3$	$-\frac{5}{12\sqrt{7\pi}} e\langle r^4 \rangle$	$+\frac{5}{12\sqrt{7\pi}} e\langle r^4 \rangle$	$-\frac{\sqrt{5}}{4\sqrt{21\pi}} e\langle r^4 \rangle$
$l = 5$ *a*	$+\frac{5}{12\sqrt{11\pi}} e\langle r^6 \rangle$	$-\frac{5}{12\sqrt{11\pi}} e\langle r^6 \rangle$	$+\frac{\sqrt{5}}{\sqrt{231\pi}} e\langle r^6 \rangle$
b	$+\frac{\sqrt{5}}{4\sqrt{77\pi}} e\langle r^6 \rangle$	$-\frac{\sqrt{5}}{4\sqrt{77\pi}} e\langle r^6 \rangle$	

[a] The wavefunctions are defined according to the standard symmetry conventions of Griffith (see [31], Tables A20 and A24)

[b] Only $i = j$ elements are allowed. The z components of the spherical harmonic functions are defined in Table 1. From these the x components may be obtained following the standard symmetry conventions

of the allowed tensor operators is

$$\begin{aligned} 0 &\to A_{1g}, \\ 2 &\to E_g + T_{2g}, \\ 4 &\to A_{1g} + E_g + T_{1g} + T_{2g}. \end{aligned} \tag{37}$$

As can be seen from this subduction scheme, a $d-d$ transition of T_{1g} symmetry, requires an operator of tensorial rank 4. Obviously, the only terms in the dynamic crystal-field hamiltonian that may couple with the electric dipole to yield such an overall hexadecapole are the $l = 3$ and $l = 5$ terms. The important lowest order $l = 1$ term, which only occurs for t_{1u} modes (see Table 2), cannot contribute to the vibronic intensity. As a result there will be no difference between t_{1u} and t_{2u} modes as far as the multipolar character of the vibronic coupling operator is concerned. Manson thus concluded that for $A_{2g} \leftrightarrow T_{2g}$ (and $A_{1g} \leftrightarrow T_{1g}$) transitions, t_{1u} and t_{2u} vibrations will give rise to comparable vibronic intensities [42]. It must be noted though that such a qualitative symmetry analysis does not allow one to predict relative vibronic intensities. Such a prediction requires a more detailed comparison of the multipole composition of each allowing mode. A first mechanism only considers the $l = 3$ terms. Subsequently the $l = 5$ terms are included as well.

5.2. *The $l = 3$ terms*

Hollebone has proposed tentative multipole assignments for the vibrational modes, on the basis of their apparent nodal structure [43]. He concluded that the t_{1u} stretching mode resembles a dipole, while both the t_{1u} and t_{2u} bending modes are predominantly octupolar. Under the assumption that the $l = 5$ terms are negligible, this assignment, in combination with the foregoing symmetry analysis, predicts that the ν_3 mode cannot induce a $d-d$ transition of T_{1g} symmetry [44]. At present a critical examination of this octupole based selectivity is apparently in order.

As a matter of fact, from the viewpoint of dynamic crystal field theory, there is no need to appeal to the type of pictorial arguments used by Hollebone, since the multipolar character of a given vibration can be determined directly from its crystal field expression. Hence the octupole field of the t_{1u} and t_{2u} modes will be given simply by the $l = 3$ term in the multipole expansions of Eqs. (13) and (14). As an example, the octupole coupling parameters for a Q_3 mode may be rewritten as a function of θ in the following way:

$$\begin{aligned} &\frac{a_3^A A_{3t_{1u}}^A}{\sqrt{m}} + \frac{a_3^B A_{3t_{1u}}^B}{\sqrt{m}} + \frac{a_3^C A_{3t_{1u}}^C}{\sqrt{M}} \\ &\quad = -\frac{2\sqrt{\pi}|q_L|e^2}{R_0^5(7mM + 14m^2)^{1/2}}\left[2\sqrt{2}\cos\theta\,\frac{2M + 7m}{\sqrt{M}} + 3\sin\theta(M + 6m)^{1/2}\right]. \end{aligned} \tag{38}$$

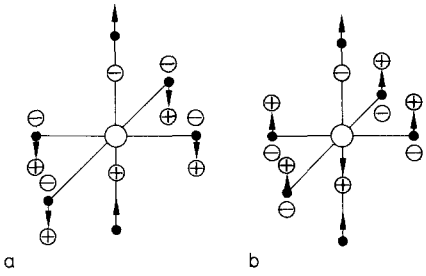

Fig. 4. Schematic representation of ligand motions with minimal ($l = 1$) (**a**) and maximal ($l = 3$) (**b**) octupole character. The + and − signs indicate regions of increasing and decreasing crystal field strength respectively. The $l = 1$ motion with minimal octupole character concentrates all charges on one pole and therefore gives rise to a dipolar field. On the other hand, the $l = 3$ motion is seen to generate an electric octupole. Clearly either motion contains both bendings and stretchings and therefore cannot coincide with the usual normal modes

This function will vanish for the θ_0 angle, given in Eq. (39), and reaches its extremal value for $\theta_0 \pm \pi/2$.

$$\tan \theta_0 = -\left(\frac{8(2M + 7m)^2}{9M(M + 6m)}\right)^{1/2}. \tag{39}$$

The θ_0 values for the complexes under consideration are included in Table 5. They all lie in a narrow range between $-60°$ and $-70°$. In Fig. 4 ligand motions with maximal and minimal octupole character are displayed. It is evident from these drawings that this multipole classification does not coincide with a separation of bending and stretching character [45]. This is further illustrated by the numerical results in Table 5, which clearly show a large gap between the θ_0 values and the typical angles of the UBFF and GHFF (θ_A) calculations. Interestingly, the only θ values in Table 5 that are close to θ_0 are the B-type solutions of the GHFF. However we recall that these do not appear to occur in nature. Hence, and as opposed to Hollebone's assumption, the actual Q_3 modes are not characterized by a weak octupole term. On the contrary they usually give rise to a somewhat stronger octupole contribution than the Q_4 mode, as may be seen by inserting the respective θ and $\theta + \pi/2$ values in Eq. (38). We therefore must conclude that an octupole based mechanism cannot explain the weakness of the ν_3 origin.

5.3. Inclusion of the $l = 5$ terms

Since the $l = 3$ terms do not give rise to the observed vibronic selectivity, a further study of the possible role of the $l = 5$ terms is needed. Combination of the expressions for the dynamic coupling constants in Table 2 and the electronic matrix elements in Table 8, yields the following general intensity formulae, as a

function of the angle θ:

$$I_3 \propto \frac{1}{\omega_3}\left[\left(\cos\theta\sqrt{\frac{2m}{(M+2m)M}}+\sin\theta\sqrt{\frac{M+6m}{(M+2m)4m}}\right)f+\cos\theta\sqrt{\frac{M+2m}{2mM}}\,g\right]^2,$$

$$I_4 \propto \frac{1}{\omega_4}\left[\left(\cos\theta\sqrt{\frac{M+6m}{(M+2m)4m}}-\sin\theta\sqrt{\frac{2m}{(M+2m)M}}\right)f-\sin\theta\sqrt{\frac{M+2m}{2mM}}\,g\right]^2,$$

$$I_6 \propto \frac{1}{\omega_6}\left[\frac{1}{\sqrt{4m}}f\right]^2,$$

with

$$f = |q_L|e^3\left(\frac{5}{7}\frac{\langle r^4\rangle}{R_0^5}+\frac{10}{11}\frac{\langle r^6\rangle}{R_0^7}\right)$$

and

$$g = |q_L|e^3\left(\frac{20}{21}\frac{\langle r^4\rangle}{R_0^5}-\frac{10}{11}\frac{\langle r^6\rangle}{R_0^7}\right). \tag{40}$$

In this equation the quantities $\langle r^4\rangle$ and $\langle r^6\rangle$ represent radial integrals over the d function. The $\langle r^4\rangle$ integral can be obtained directly from the spectrochemical strength Dq:

$$Dq = \frac{|q_L|e^2\langle r^4\rangle}{6R_0^5}. \tag{41}$$

On the other hand, the $\langle r^6\rangle$ integral does not occur in expressions for the static ligand field of d electrons. While it is sometimes assumed that this integral is much smaller [46] than $\langle r^4\rangle$, it can be argued that — exactly as in the case of the static ligand field theory — attempts to calculate such integrals *ab initio* are deemed to fail as a result of the many approximations of the electrostatic model. Hence we consider the ratio $\varrho = \langle r^6\rangle/R_0^2\langle r^4\rangle$ as a new dynamic parameter, to be determined from experiment. In Fig. 5 the relative intensities $I_4 : I_3$ and $I_6 : I_3$ are plotted as a function of ϱ for the case of MnF_6^{2-}, taking the θ from the UBFF. The figure confirms the earlier results that for $\varrho = 0$, i.e. in the absence of $l = 5$ terms, there is no vibronic selectivity. However with increasing values of ϱ vibronic intensity is rapidly concentrated [47] in the ν_6 and ν_4 false origins, in qualitative agreement with the experimental selectivity. Indeed if the $l = 3$ and $l = 5$ terms are of comparable magnitude, the f function in Eq. (40) will be much larger than the g function. As a result the bending modes, with a predominant f dependence, will gain intensity while the stretching mode, which is dominated by g, will be weakened. For ϱ larger than 3 the selectivity decreases again, as the $l = 5$ term becomes gradually more important. Consequently the observed selectivity must be attributed to the combined effect of the $l = 3$ and $l = 5$ terms in the dynamic crystal field operator.

Finally we note that there is only one semi-empirical parameter ϱ to fit two independent intensity ratios $I_4 : I_3$ and $I_6 : I_3$. The point-charge electrostatic model of the dynamic ligand field thus appears to be underparametrized. This is in

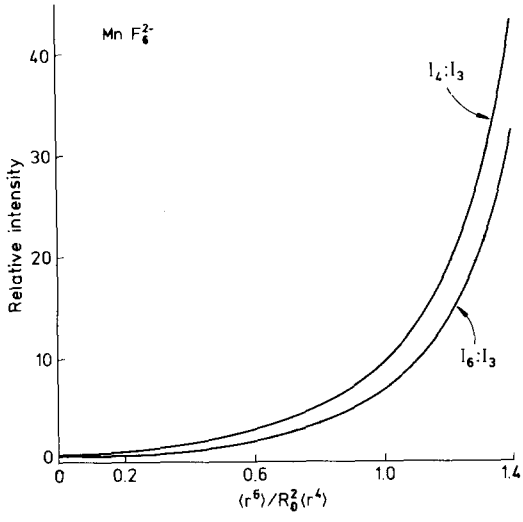

Fig. 5. Relative intensities of the vibronic side bands in MnF_6^{2-}, plotted as a function of $\varrho = \langle r^6\rangle/R_0^2\langle r^4\rangle$. The functions were calculated from Eq. (40), using the UBFF angle $\theta = -7°$. Selectivity is absent for $\varrho = 0$ ($I_4 : I_3 = 0.6$, $I_6 : I_3 = 0.3$). For $\varrho \geqslant 1$ most intensity is concentrated in the side bands of the bending modes

marked contrast with the static crystal field model, where there is one potential operator parameter, $10Dq$, for exactly one phenomenological energy difference between e_g and t_{2g} orbitals [48].

6. Conclusions

(i) There is little doubt that the separation of the odd t_{1u} vibrations in an octahedral complex follows a stretching-bending splitting, rather than a dipole-octupole one. The evidence comes from concurring results of the UBFF and GHFF (θ_A) calculations. The alternative GHFF θ_B solution must be rejected as being unphysical.

(ii) Selective vibronic coupling to the ν_4 and ν_6 bending modes cannot arise via the octupole terms, but is due to the combined effect of the $l = 3$ and $l = 5$ terms. In the intensity expressions for the ν_3 stretching mode these contributions tend to cancel.

(iii) The role of the force field in the intensity calculations is contained in the angular parameter θ. Extensive comparison of different force fields has shown that this parameter is confined to a narrow range (cf. Table 5). Therefore we can eliminate the possibility of a critical dependence of the intensity calculations on the choice of force field.

(iv) It should be kept in mind that our conclusions were derived from a simple electrostatic model, using the closure procedure. Alternative or complementary models are available, involving d–p mixing as a source of intensity [1] and dynamic contributions from the ligand polarization mechanism [49–51].

Acknowledgements. The authors thank C. D. Flint, R. Acevedo, H.-H. Schmidtke, H. Kupka and J. Degen for discussion and correspondence. A.C. is indebted to the Belgium National Science Foundation (NFWO) and the Belgian Government (Programmatie van het Wetenschapsbeleid) for financial support.

References and notes

1. Liehr AD, Ballhausen CJ (1957) Phys Rev 106:1161
2. Koide S, Pryce MHL (1959) Phil Mag 3:607
3. Faulkner TR, Richardson FS (1978) Mol Phys 35:1141
4. Judd BR (1980) Physica Scripta 21:543
5. Satten RA, Schreiber CL, Wong EY (1983) J Chem Phys 78:79
6. Kupka H, Wernicke R, Ensslin W, Schmidtke, H-H (1979) Theor Chim Acta 51:297
7. Acevedo R, Flint CD (1983) Mol Phys 49:1065
8. Ballhausen CJ (1989) In: Flint CD (ed) Vibronic processes in inorganic chemistry. NATO ASI Series; Kluwer, Dordrecht
9. See e.g.: Butler PH (1981) Point group symmetry applications. Plenum Press, New York, Table 16.2, p 520
10. Independence of subrepresentations is only guaranteed if the component labels for the symmetry coordinates and for the Y functions are defined according to the same symmetry relations
11. Acevedo R, Meruane T, Letelier, JR (1984) Theor Chim Acta 64:339
12. Liehr AD, Ballhausen CJ (1958) Ann Phys 3:304
13. Kim H, Souder PA, Claassen HH (1968) J Molec Spectrosc 26:46. Note that in Eq. (1) of this paper a minus sign is lacking in front of the summation sign. In Eq. (4) the sum $\Sigma\, \Delta\alpha_{ij}$ should be replaced by $\Sigma\, (\Delta\alpha_{ij})^2$
14. Wilson EB, Decius JC, Cross PC (1955) Molecular vibrations. McGraw-Hill, New York, pp 56–58
15. Kupka H (1978) Mol Phys 36:685
16. The frequency denominator in Eq. (28) stems from the vibrational integral $\langle 0|Q|1\rangle^2$. For a mass-weighted normal coordinate, one has $\langle 0|Q|1\rangle^2 = \hbar/2\omega = \hbar/4\pi cv$, where v is the frequency in wave numbers
17. Ceulemans A, Beyens D, Vanquickenborne LG (1982) J Am Chem Soc 104:2988
18. Ceulemans A, Bongaerts N, Vanquickenborne LG (1987) Inorg Chem 26:1566
19. Flint CD (1974) Coord Chem Rev 14:47
20. Greenough P, Paulusz AG (1979) J Chem Phys 70:1967
21. Dubicki L, Ferguson J, van Oosterhout B (1980) J Phys C 13:2791
22. Denning RG (1989) In: Flint CD (ed) Vibronic processes in inorganic chemistry. NATO ASI Series; Kluwer, Dordrecht
23. Pfeil A (1971) Theor Chim Acta 20:159
24. Chodos SL, Black AM, Flint CD (1976) J Chem Phys 65:4816
25. Kozikowski BA, Keiderling TA (1980) Chem Phys 53:323
26. Flint CD, Greenough P (1972) J Chem Soc Faraday Trans 2 68:897
27. Urushiyama A, Schönherr T, Schmidtke H-H (1986) Ber Bunsenges Phys Chem 90:1188
28. Flint CD, Paulusz AG (1981) Mol Phys 44:925
29. Flint CD, Lang PF (1986) J Chem Soc Faraday Trans 2 82:465
30. Lomenzo J, Patterson H, Strobridge S, Engstrom H (1980) Mol Phys 40:1401
31. Griffiith JS (1964) The theory of transition-metal ions. Cambridge University Press, London, p 419
32. Hoggard PE (1986) Coord Chem Rev 70:85
33. Güdel HU, Snellgrove TR (1978) Inorg Chem 17:1617
34. Knochenmuss R, Reber C, Rajasekharan MV, Güdel HU (1986) J Chem Phys 85:4280
35. Labonville P, Ferraro JR, Wall MC, Basile LJ (1972) Coord Chem Rev 7:257
36. O'Leary GP, Wheeler RG (1970) Phys Rev B 1:4409

37. Pistorius CWFT (1958) J Chem Phys 29:1328. In the potential function of this reference $2d^2f_\alpha$ should be replaced by d^2f_α, and a term $2d^2f_{\alpha\alpha''}\,\Delta\alpha_{45}\,\Delta\alpha_{23}$ should be added
38. Weinstock B, Goodman GL (1965) Adv Chem Phys 9:169
39. Hoy AR, Stone JMR, Watson JKG (1972) J Molec Spectrosc 42:393
40. McDowell RS, Asprey LB (1973) J Molec Spectrosc 48:254
41. McDowell RS, Asprey LB, Paine RT (1974) J Chem Phys 61:3571
42. Manson NB (1975) J Phys C 8:L483
43. Hollebone BR (1980) Theor Chim Acta 56:45
44. Ceulemans A (1983) Chem Phys Lett 97:365
45. For a group-theoretical discussion of the t_{1u} multiplicity problem, see: Lulek T (1980) Acta Phys Polonica A 57:407; Ceulemans A (1985) Mol Phys 54:161
46. Manson NB (1971) Phys Rev B 4:2645
47. In [7] the relative intensities of the bending modes were calculated to *decrease* with increasing values of ϱ. As we have argued in Sect. 2, these results can be shown to be in error as a consequence of the use of an erroneous coordinate transformation
48. Newman DJ, Chen SC (1982) Phys Rev B 25:41
49. Mason SF (1979) Accounts Chem Res 12:55
50. Meruane T, Acevedo T (1983) Theor Chim Acta 62:301
51. Acevedo R, Flint CD (1984) Mol Phys 53:129; (1985) ibid. 56:683